# Steer By Wire Control System

Omar Shibli *Electric and Computer Engineering*
*American University of Beirut*
ois02@mail.aub.edu
Omar Mardini *Electric and Computer Engineering*
*American University of Beirut*
ojm04@mail.aub.edu
Nadim Succar *Electric and Computer Engineering*
*American University of Beirut*
nks16@mail.aub.edu

The aim of this report is to design a steer by wire control system for a Beirut-based electric motor controller manufacture, "MC Lebanon". Throughout the report, requirements presented by the company are discussed in order to extract controller specifications, and identify constraints sets on the project.

## I. Literature Review

### A. Introduction

In the realm of automotive engineering, steer-by-wire (SbW) is an emerging technology that transforms the current mechanical steering system into an electronic system. Steering systems are traditionally reliant on mechanical linkages from the steering wheel to the steering gear, all the way to the front wheel. Beyond the technological nuances, SbW systems promise far-reaching benefits in the automotive world. They allow for easy customization, enhanced handling, and additional safety features at the cost of maintenance and power costs. However, as the automotive industry continues to move towards electronic systems and the computerization of cars, the integration of SbW systems represents a brighter future in vehicular steering systems.

### B. Principles of Steer-by-wire

A steer by wire system is a technology that opts to eliminate the mechanical connection between the steering wheel and the wheels themselves. Usually, a traditional steering system uses a rack and pinion to convert the rotational movement of the steering wheel to linear motion in the wheels. At the end of the steering shaft, which is connected to the steering wheel, is a pinion. This pinion is a small gear that turns with the steering wheel. Its teeth are connected to the teeth of the rack which is a long metal rod that turns left and right in response to the pinion's rotation. This sideways movement pushes on the wheels to cause them to rotate and therefore steer.

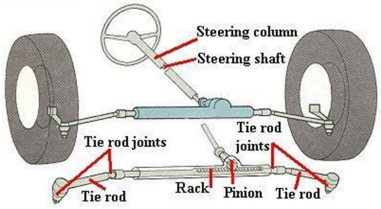


Fig. 1. Rack and Pinion steering mechanism.

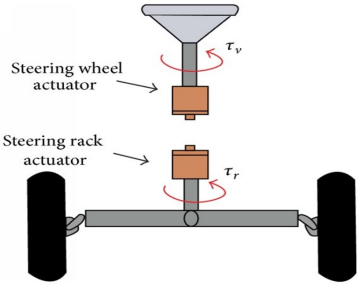


Fig. 2. Steer by wire mechanism

On the other hand, a steer-by-wire system eliminates all the mechanical linkages by a simple wire connected between two DC motors at each end. It communicates by sending electronic signals and sensors to transmit the driver's input to the wheels. Furthermore, steer-by-wire systems provide many benefits to the automotive industry. Steer-by-wire systems allow for customization, which proves useful when it comes to the accommodation of disabled people as the steering wheel will no longer hold to the constraints of mechanical linkage. Traction control systems can also benefit from a steer-by-wire system as it can override the natural instincts of drivers and perform the needed maneuvers to take control if the situation goes awry. However, the benefits of steer-by-wire systems come at the expense of maintenance and power cost as steer-by-wire systems require more power than conventional systems. In addition, its all-electric nature can open the possibility of more electrical failures.

### *C. Controllers*

In similar steer-by-wire projects, PID controllers are used for the steering wheel and front wheel system. The PID controller in that case is responsible for the adjustment of the steering angle to its desired value when it calculates the error. Initially, their response is unstable, but by using the PID controller, the system is stabilized regardless of the existence of any disturbances at the input of the system. This control strategy improves the maneuverability and stability of their system. In a comparative study for DC motor position controllers, PIDs are also studied. It is determined that PID controllers are popular because of their performance and the simplicity of their parameters, however, PIDs cannot work with more rigorous systems or with systems with an order higher than two, and they can be affected by the physical deterioration of elements, noise, or load disturbance. The PID controllers are implemented using a PIC microcontroller. PIC microcontrollers are meant to fit in embedded systems and allow interfacing with the system. In this case, the PIC microcontroller is used to process the outputs from the rotary sensors. Then, they use a KBBC-24M as a motor controller for the steering actuator. The KBBC-24M is part of a series of

battery powered DC motors which is able to provide specific tailoring to their application.

In "Modelling and Simulation of Vehicle Steer by Wire System", a paper from the University of Technology Malaysia, their design of the control structure consists of the steering wheel system, the front wheel system, and the controller, all of which are modelled according to Newton's Law. Each of the steering systems has their own separate PID controller that adjusts the steering wheel angle to a desired angle when the error is calculated.

In "Research on Control Strategies of Steer-By-Wire System", a paper from the School of Electronic Information Control Engineering, a more advanced test platform is implemented where it is separated into three parts, a dSpace, a steering bench, and a wheels bench, all of which are connected to the controller. In this part of the research, dSpace is a software responsible for the distribution of data. Moreover, with the input from the steering wheel, the sensor signal from the steering bench moves to the controller along with the current angle of the wheels bench by way of dSpace. Through this, all the information gets sent and dealt with accordingly in order to rotate the wheels.

## II. Customer Specifications

Before working on this project, it is important to understand the desired outcomes of our work. This includes taking a look at the customers specifications and extracting the technical and non-technical constraints.

### A. Non-technical Constraints

"MC Lebanon" set both a deadline and a budget constraint for this project. The project is to be finalized within 3 weeks and with a budget that is no more than a $1000 dollars.

### B. Technical Constraints

Since the controller aims to control a steering system, it is important to ensure safety and proper functioning of the system. The customer asks for the steering actuator to stop at most $\pm$ 2 °, and should reach that angle within 0.25 seconds. In addition to that, their engineers have found that the steering mechanism must not exceed 5 °of the intended angles set by the steering wheel.
These constraints can be interpreted as limitations for maximum overshoot, steady-state error, and settling time. During preliminary research, we have found that, on average, cars have a 35 °wheel steering angle.

*1) Maximum Overshoot:* To find the maximum overshoot:

$$M_p = \frac{40 - 35}{35} \times 100 = 13.28 \tag{1}$$

This can be used to find the damping ratio ($\zeta$) for our desired system by:

$$0.1428 = e^{(\frac{\zeta}{\sqrt{1-\zeta^2}})\pi} \tag{2}$$

$$=> \zeta = 0.527$$

*2) Settling Time:* The settling time ($t_s$ is also given as 0.25 seconds which can be used to derive the natural frequency of the desired system:

$$w_n = \frac{4}{t_s \zeta} \tag{3}$$

$$=> w_n = 30.36 rad/s$$

## III. Dynamic Model

First, it is important to model the electric and mechanical systems of the servo in order to understand the system at hand. This is done through a transfer function and state space

representation. There are two equations that govern the system given as:

$$J\ddot{\theta} + b\dot{\theta} = Ki \tag{4}$$

$$L\frac{di}{dt} + Ri = V - K\dot{\theta} \tag{5}$$

Using Laplace Transform:

$$(Js^2 + bs)\theta(s) = KI(s) \tag{6}$$

$$(Ls + R)I(s) = V(s) - Ks\theta(s) \tag{7}$$

### A. Transfer Function:

In the mathematical equations, $\theta(s)$ will be considered as the output and V(s) as the input. I(s) will be eleminated from both equations 3 and 4 and they will equated to each other.

$$\frac{(Js^2 + bs)\theta(s)}{K} = \frac{V(s) - Ks\theta(s)}{Ls + R} \tag{8}$$

$$=> \theta(s)(\frac{Js^2 + bs}{K} + \frac{Ks}{Ls + R}) = \frac{1}{Ls + R}V(s)$$

$$=> \frac{\theta(s)}{V(s)} = \frac{\frac{1}{Ls+R}}{\frac{Js^2+bs}{K} + \frac{Ks}{Ls+R}}$$

This equation is simplified to attain the final form:

$$\frac{\theta(s)}{V(s)} = \frac{\frac{K}{JL}}{s^3 + \frac{(JR+bL)}{JL}s^2 + \frac{Rb+K^2}{JL}s} \tag{9}$$

### B. State Space Representation

Next, the state space representation should be derived.

$$\text{KV(s)} = \text{JL}s^3\theta(s) + (JR + bL)\theta(s) + (Rb + K^2)s\theta(s) \tag{10}$$

Inverse Laplace transform is applied:

$$\text{Kv(t)} = \text{JL}\dddot{q}(t) + (JR + bL)\ddot{q}(t) + (Rb + K^2)\dot{q}(t) \tag{11}$$

$$x_1 = \dot{q}(t) \tag{12}$$

$$x_2 = \dot{x}_1 = \ddot{q}(t) \tag{13}$$

$$\dot{x}_2 = \dddot{q}(t) \tag{14}$$

Equations 9, 10, and 11 are replaced in equation 8.

$$Kv(t) = JL\dot{x}_2 + (JR + bL)x_2 + (Rb + K^2)x_1$$

$$\begin{bmatrix}\theta \\ \dot{\theta} \\ i\end{bmatrix} = \begin{bmatrix}0 & 1 & 0 \\ 0 & \frac{-b}{J} & \frac{K}{J} \\ 0 & \frac{-K}{L} & \frac{-R}{L}\end{bmatrix}\begin{bmatrix}\theta \\ \dot{\theta} \\ i\end{bmatrix} + \begin{bmatrix}0 \\ 0 \\ \frac{1}{L}\end{bmatrix}v(t) \tag{15}$$

$$v(t) = \begin{bmatrix}1 & 0 & 0\end{bmatrix}\begin{bmatrix}\theta \\ \dot{\theta} \\ i\end{bmatrix} \tag{16}$$

Equations 12 and 13 are the space state equations.

### C. System Identification

Next, it is important to find the real system parameters. They can be determined by looking at the user manual of the DC servo motor in use and confirming these values by conducting experiments and collecting data through step, ramp, and impulse response. Simulink will be used to do that. In order to collect the data, the $\frac{\dot{\theta}(s)}{V(s)}$ equation was used in order to eliminate the pure integrator, and a filter was added to elimante noise due to the derivative.

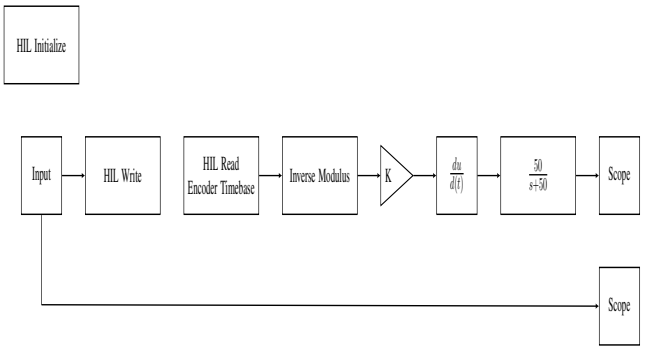


Fig. 3. Simulink setup for data acquisition

The above setup was subjected to different inputs such as a step and ramp input. The data was collected and then imported into the system identification tool provided by MATLAB. The different data files of each input were merged together, and then the tool estimated a proper transfer function fitting the data. The transfer function was:

$$\frac{\dot{\theta}(s)}{V(s)} = \frac{9098}{s^2 + 60.9s + 425.5} \tag{17}$$

After obtaining the above equation is to modify our nominal values from the DC motor sheet in order to determine the exact parameters of the system by curve fitting our values to the experimental values.

| Symbol | Description | Value |
|---|---|---|
| **DC Motor** | | |
| $V_{nom}$ | Nominal input voltage | 18.0 V |
| $\tau_{nom}$ | Nominal torque | 22.0 mN-m |
| $\omega_{nom}$ | Nominal speed | 3050 RPM |
| $I_{nom}$ | Nominal current | 0.540 A |
| $R_m$ | Terminal resistance | 8.4 Ω |
| $k_t$ | Torque constant | 0.042 N-m/A |
| $k_m$ | Motor back-emf constant | 0.042 V/(rad/s) |
| $J_m$ | Rotor inertia | $4.0 \times 10^{-6}$ kg-m$^2$ |
| $L_m$ | Rotor inductance | 1.16 mH |
| $m_h$ | Module attachment hub mass | 0.016 kg |
| $r_h$ | Module attachment hub radius | 0.0111 m |
| $J_h$ | Module attachment moment of inertia | $0.6 \times 10^{-6}$ kg-m$^2$ |
| **Inertia Disc Module** | | |
| $m_d$ | Disc mass | 0.053 kg |
| $r_d$ | Disc radius | 0.0248 m |
| **Rotary Pendulum Module** | | |
| $m_r$ | Rotary arm mass | 0.095 kg |
| $L_r$ | Rotary arm length (pivot to end of metal rod) | 0.085 m |
| $m_p$ | Pendulum link mass | 0.024 kg |
| $L_p$ | Pendulum link length | 0.129 m |
| **Motor and Pendulum Encoders** | | |
| | Encoder line count | 512 lines/rev |
| | Encoder line count in quadrature | 2048 lines/rev |
| | Encoder resolution (in quadrature) | 0.176 deg/count |
| **Amplifier** | | |
| | Amplifier type | PWM |
| | Peak Current | 2 A |
| | Continuous Current | 0.5 A |
| | Output voltage range | ±10 V |

Fig. 4. DC motor nominal values.

The above table includes all the nominal values of the coefficients used in the transfer function (eq.6).

| | |
|---|---|
| K | 0.042 $\frac{V}{(rad/s)}$ |
| L | $1.16 \times 10^{-3}$ mH |
| J | $J_m + J_h + \frac{1}{2} m_d r_d^2 = 2.1 \times 10^{-5} kg.m^2$ |
| R | 8.4 ohm |

TABLE I
NOMINAL TRANSFER FUNCTION PARAMETERS

What remains is the parameter b that can be determined using experiment. For now it can be approximated using the following equation:

$$b = \frac{I_{nom}}{w_{nom}} \times k_t = 6.88 \times 10^{-5} N.m/w \tag{18}$$

*1) Padet approximation of time delay:* When subjecting the Quanser Qube servo to a step function we notice a small time delay before the qube responds to any

input. This time delay was found to be around 0.008 seconds.

| Time (s) | Input | Output |
|---|---|---|
| 0.998 | 0 | 0 |
| 1 | 1 | 0 |
| 1.002 | 1 | 0 |
| 1.004 | 1 | 0 |
| 1.006 | 1 | 0 |
| 1.008 | 1 | 0.1534 |

TABLE II
OUTPUT DATA OBTAINED FROM THE QUBE SERVO

In the above table it is clear that the step input begins and t = 1s however the Qube does not respond until t = 1.008s. In order to reflect this time delay in our transfer function we have to use padet approximation. To determine the order of the pade approximation required to use, the frequency range of operatiion should be examined. It can be noticed when plotting the bode plot of our experimental transfer function that our 3dB frequency is around 7.85 rad/s. Then our pade approximation should correctly approximate the delay up to this value. A first order pade approximation of the 0.008 seconds is enough, so our equation becomes:

$$t_d = \frac{-0.004s + 1}{0.004s + 1} \tag{19}$$

*2) Real system parameters:* MATLAB was used to determine the real system parameters. Both the nominal transfer function and the experimental transfer function were subjected to step responses, and the nominal values were adjusted to fit the nominal trasnfer function to the experimental. Upon starting the curves looked as follows:

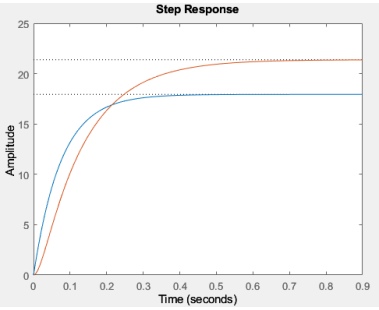


Fig. 5. Nominal and experimental plots before adjustments.

When calculating the roots of the transfer function it becomes clear that J moves both poles, meaning it affects both the gain and the speed of the slow pole while R, b, and K will affect only the gain of the transfer function. In this case J will be used to adjust the speed of the pole and fixing the transient response, and R, b, and K will be used to adjust the gain and steady state error. When adjusting the afformentioned values we are able to fit the curve exactly, the parameters become:

| Parameter | Value | Percent error |
|---|---|---|
| K | 0.039 $\frac{V}{(rad/s)}$ | 7% |
| L | $1.16 \times 10^{-3} mH$ | 0% |
| J | $3.2 \times 10^{-5} kg.m^2$ | 9% |
| R | 7.5 ohm | 10.7 % |
| b | $4 \times 10^{-5}$N.m/w | -% |

TABLE III
NOMINAL TRANSFER FUNCTION PARAMETERS

After the adjustments shown above it can be sees how close the two graphs become:

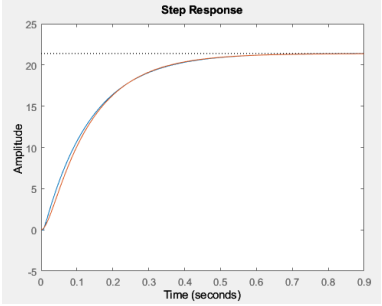


Fig. 6. Nominal and experimental plots after adjustments.

Therefore our transfer function becomes:

$$G(s) = \frac{-0.004s + 1}{0.004s + 1} \times \frac{1.015 \times 10^6}{s^3 + 6467s^2 + 4.906 \times 10^4 s} \tag{20}$$

## IV. Analysis

### A. Open-Loop Analysis

Open-Loop Transfer Function:
$\frac{-4203s+1.051*10^6}{0.004s^4+26.87s^3+6663s^2+4.906*10^4 s}$

*Time Domain Analysis:* After the proper analysis on MATLAB, overshoot, settling time, and steady-state error provides with NaN results. This indicates the instability of the system as its output diverges without bound when it subjected to the step input.

*Frequency Domain Analysis:* Concerning the frequency domain analysis, the resulting values of the phase margin, gain margin, and bandwidth were all positive with respective values of 27.5845, 5.8102, and 30.2818. In addition, since the system is unstable, the gain margin indicates how much the gain should be decreased to make it stable, in this case by a value of 301.8754.

The bode plot shows multiple corner frequencies as the corresponding magnitude plot and phase plot change. In the case of the phase plot, it drops from 270° to -90°. Moreover, the Nyquist plot shows no encirclement of the (-1, 0) point on the complex plane.

Finally, only the observability provides full rank. This suggests that the system is observable but may not be controllable in all states.

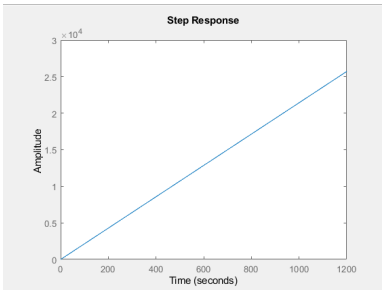


Fig. 7. Open loop step response

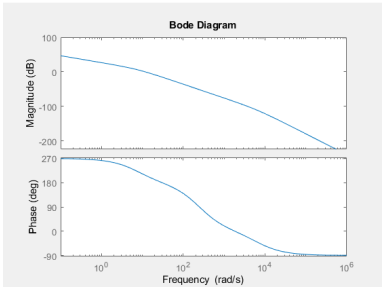


Fig. 8. Open loop bode plot

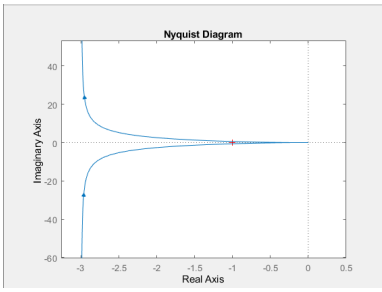


Fig. 9. Open loop nyquist plot

### B. Closed-Loop Analysis

Closed-Loop Transfer Function:

$$\frac{-2101500+525.5*10^6}{2s^4+13435s^3+3331500s^2+22428500s+525.5*10^6}$$

*Time Domain Analysis:* The system provides the following values of overshoot, settling time, and steady-state error: 45.1489, 1.1201, and 0.7959. The system exhibits a high overshoot and a slow settling time with respect to customer specifications. There is also a steady-state error which poses a discrepancy between the desired and actual outputs.

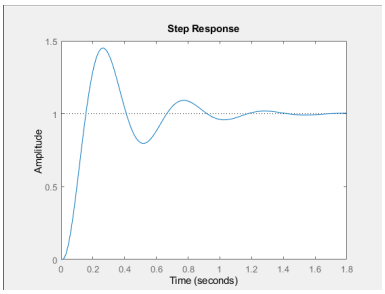


Fig. 10. Closed loop step response

*Frequency Domain Analysis:* The resulting values of phase margin, gain margin, and bandwidth after frequency domain analysis are respectively: 32.7160, 4.8102, and 30.2819. The phase margin and gain margin both being positive is a good indicator towards stability. In addition, the magnitude plot of the bode plot shows a peak in magnitude at 11 rad/s. This corresponds to the resonant frequency $w_r = 11rad/s$. The Nyquist plot shows no encirclement of the (-1, 0) point in the complex plane.
Finally, in regards to the controllability and observability, only the observability matrix provides full rank. This shows that the system is observable but might not be controllable in all states.

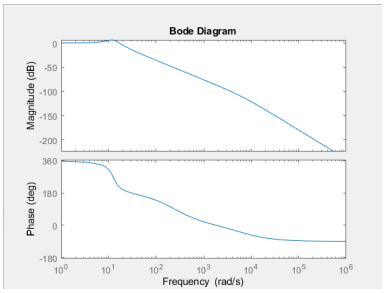


Fig. 11. Closed loop bode plot

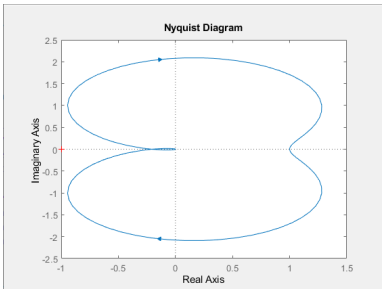


Fig. 12. Closed loop nyquist plot.

## V. Design Alternatives

In this part of the report, different controllers will be discussed and evaluated in order to stabilize the system.

### A. Proportional Controller

To design a proportional controller we have to look at the root locus of our system using our open loop transfer function

$$G(s) = \frac{-4203s + 1.051 \times 10^6}{0.004s^4 + 26.87s^3 + 6663s^2 + 4.906 \times 10^4 s} \quad (21)$$

First the root locus plot should be acquired. It is important to realize that this is a non-minimum phase system since there is a zero in the RHP. The zeros and poles on the real axis are:

| Poles | Zeros |
|---|---|
| s = 0 | s=250 |
| s = -6459.9 | |
| s = -7.6 | |
| s = -250 | |

TABLE IV
POLES AND ZEROS OF OLTF

Then the angles of the asymptotes are calculated. Since this is a nonminimum phase system the angle criterion changes and adds 180°.

$$\angle = \frac{\pm 180(2k+1)}{n-m} + 180 = \pm 120, +360 \quad (22)$$

After that it is required to find the break in points by finding:

$$\frac{dK}{ds} = 0 \quad (23)$$

The values acquired are: s = 401, s = -3.73, s = -155, s= -4386. These values can be verified using MATLAB. The root locus plot obtained through MATLAB is as in figure 13. The critical K value for which the system becomes unstable is K = 5.8. By looking at the value of $\zeta$ in the

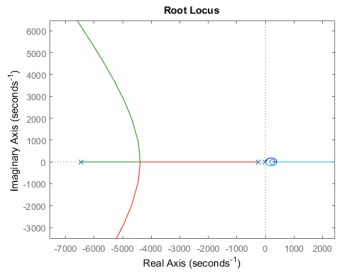


Fig. 13. Root Locus of Open-Loop Transfer Function

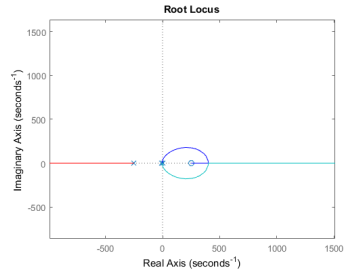


Fig. 14. Zoomed-In Root Locus

specifications, a line of constant damping can be drawn and the value of K can be determined by the intersection between the line and the root locus.

$$cos^{-1}(\zeta) = cos^{-1}(0.59) = 53.84 \quad (24)$$

This results in a K = 0.5. The closed loop transfer function response to a step input before the controller can be observed in figure 10.After adding the controller to the system, the CLTF step response can be seen in figure 15.

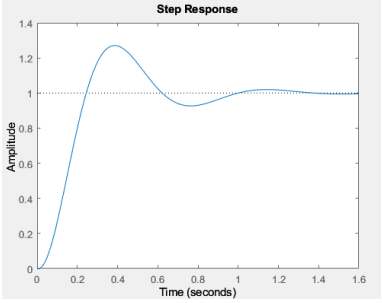


Fig. 15. K controller CLTF response to step input

It is clear that the proportional controller decreased overshoot from 45% to 27%, which is still outside the required specifications, settling time also decreased from 1.12s to 0.94s which is also still higher than the specifications (0.25s). If the controller value is decreased past this point, it will decrease the overshoot to within accepted levels but would hurt the settling time. It is also noticeable that the step response has 0 steady state error due to the pure integrator in the plant.

### B. Lead Compensator

*1) First Iteration:* When looking at the closed loop response of the transfer function, it is clear that the overshoot and the settling time should be reduced. The root locus of the system has already been plotted previously in the proportional controller. Our desired closed loop poles are $s = -16 \pm j25.8$, and are found by using $s = -\zeta w_n \pm w_n\sqrt{1-\zeta^2}$. The deficiency angle can be found by $\phi = 180 - \angle\frac{-4203s+1.501*10^6}{0.004s^4+26.87s^3+6663s^2+4.906*10^4} = 61.9\ °$. The zero can be taken at s = -16.

$$tan(61.9) = \frac{opp}{25.8} \tag{25}$$

$$=> opp = 46.76$$

$$=> s = 46.76 + 16 = 62.76$$

The lead compensator equation becomes

$$G_c = K_c\frac{s+16}{s+62.76} \tag{26}$$

To find the value of $K_c$ :

$$|K_c(\tfrac{s+16}{s+62.76})(\tfrac{-4203s+1.501\times10^6}{0.004s^4+26.87s^3+6663s^2+4.906\times10^4})| = 1 \tag{27}$$

$$=> K_c = 9.615$$

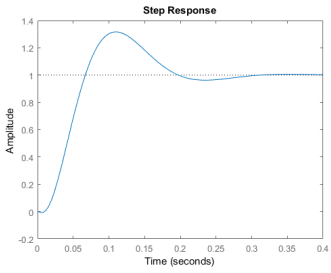


Fig. 16. Step Response of First Lead Compensator Iteration

It is clear that the overshoot remains high compared to the desired specification. The values that are obtained from figure 16 are overshoot of 31.6% and a settling time of 0.27 seconds. These values do not meet the requirements, then another iteration is needed in order to obtain better values.

*2) Second Iteration:* The attempt for this iteration is to try moving the pole and the zero to the right in order to decrease the overshoot. Take s = -7.615. In order to satisfy the deficiency angle, the pole is taken at s = -42.76. To find $K_c$:

$$|K_c(\tfrac{s+7.617}{s+40.83})(\tfrac{-4203s+1.501\times10^6}{0.004s^4+26.87s^3+6663s^2+4.906\times10^4})| = 1 \tag{28}$$

$$=> K_c = 5.85$$

The compensator equation becomes

$$G_c(s) = 5.85(\frac{s+7.617}{s+40.83}) \tag{29}$$

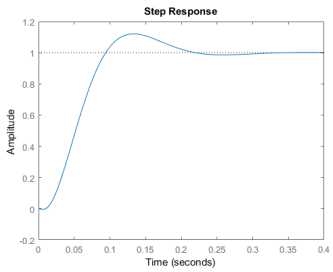


Fig. 17. Step response of Second Lead Compensator Iteration

When looking at figure 17, it can be deduced that the values have improved significantly. The overshoot is 12% and the settling time is 0.2 seconds; both of these values are within the specified requirements. However, this compensator cannot be used as experimentally it displayed significant steady-state error. This behavior is expected due to the absence of a lag compensator paired with the system.

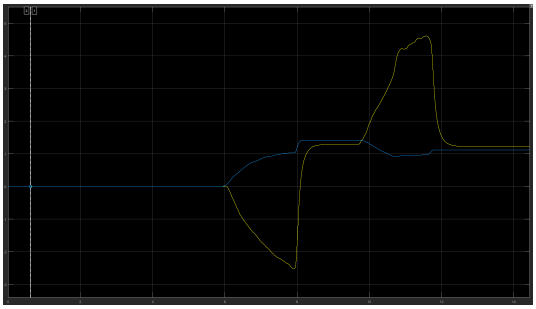

Fig. 18. Experimental Response

As can be seen in figure 18, the response displays significant steady-state error measured at 3.7 °. This exceeds the specifications set at 2 °steady-state error.

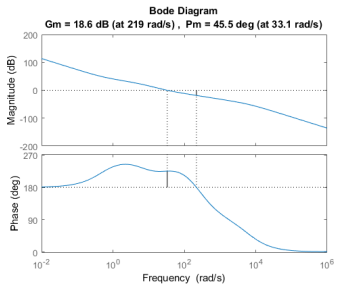


Fig. 19. Bode Plot of PID-compensated transfer function

## C. PID Controller

This sections attempts to create a PID controller for the system. The desired pole remains the same at $s = -16 + j25.8$. and so does the deficiency angle at $\phi = 61.9$.

$$\frac{25.8}{s-16} = tan(61.9) => s = -29.77 \tag{30}$$

The equation of the controller becomes

$$K_c(s+29.7) \tag{31}$$

To find the gain $K_c$

$$|K_c(s+29.7)(\frac{-4203s+1.501\times10^6}{0.004s^4+26.87s^3+6663s^2+4.906\times10^4})| = 1 \tag{32}$$

$=> K_c = 0.15$

For the PI portion, the integrator is chosen close to the jw axis.

$$G_{PI}(s) = \frac{s+0.01}{s} \tag{33}$$

With the adjusted gain, the PID controller becomes

$$G_{PID}(s) = 0.1537(s+29.7)(\frac{s+0.01}{s}) \tag{34}$$

The equation is expanded in order to get the $K_p, K_i,$ and $K_d$ values.

$$G_{PID}(s) = \frac{0.1537s^2+5s+0.05}{s} \tag{35}$$

## VI. Final Design

The PID represented in equation 35 is used as the final design for our controller. This is because the controller displays a proper response to the input signals which are demonstrated in figures 20, 21, and 22.

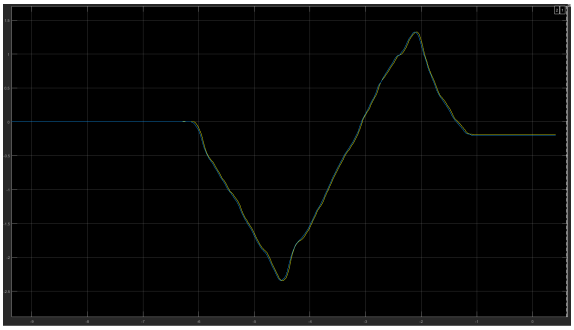

Fig. 20. Experimental Response 1

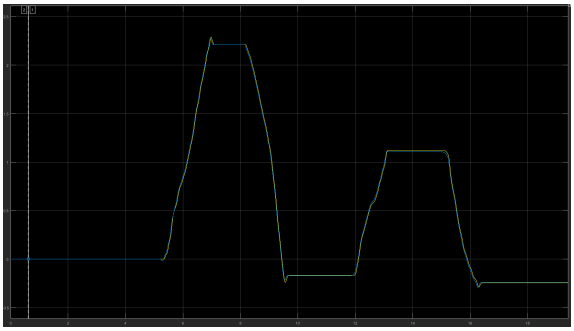

Fig. 21. Experimental Response 2

In figure 20 and 21, it can be seen that the response follows the master accurately with an error of 0.21%. This is in line with the specifications as it demonstrates nearly no overshoot and a near zero steady state error. Also, the settling time for this system is measured at 0.19 seconds.

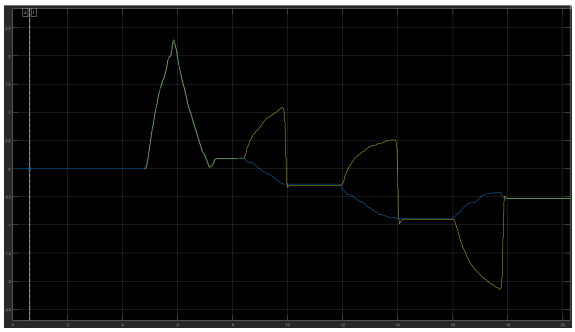

Fig. 22. Experimental Response with Disturbance

In figure 22, the response of the cube servo is seen with outside disturbances. The slave servo is held in place while the master is moved, the force of the servo rotation can be strongly felt when held in place. In addition to that, the response displays near zero steady state error after the slave servo is released. This shows proper error correction and the proper functioning of the integral in the system. The response does not display much overshoot as it does not exceed 12%.

## VII. Conclusion

After many attempts at designing a proper controller for the system at hand, it can be said that many designs could be an effective solution for this system. The lead compensator is very close to attaining the system specifications. However, it fails to maintain a good steady-state error. In order to fix this issue, a PID controller is designed instead; it meets all design requirements by maintaining a 14% maximum overshoot, zero steady-state error, and a decent settling time of less than 0.23 seconds as a worst case estimation. Finally, it can be said that a proper controller is designed, simulated, and tested to meet all constraints set forward on the project.

## VIII. References

[1] Kader, A. (2006, May). Steer-by-Wire Control System.

[2] Fahami, S. M., Zamzuri, H., Mazlan, S. A., amp; Zakaria, M. A. (2012). Modeling and simulation of vehicle steer

by Wire System. 2012 IEEE Symposium on Humanities, Science and Engineering Research. https://doi.org/10.1109/shuser.2012.6268992
[3] Flores Moran, M. E., amp; Aracely Pozo Viera, N. (2017). Comparative study for DC motor position controllers. 2017 IEEE Second Ecuador Technical Chapters Meeting (ETCM). https://doi.org/10.1109/etcm.2017.8247475
[4] Jianmin, D., Ran, W., amp; Yongchuan, Y. (2010). Research on control strategies of steer-by-wire system. 2010 International Conference on Intelligent Computation Technology and Automation. https://doi.org/10.1109/icicta.2010.238
[5] Bacac, N., Slukic, V., Puskaric, M., Stih, B., Kamenar, E., amp; Zelenika, S. (2014). Comparison of different DC motor positioning control algorithms. 2014 37th International Convention on Information and Communication Technology, Electronics and Microelectronics (MIPRO). https://doi.org/10.1109/mipro.2014.6859832
[6] Khushboo Sao, amp; Dr. Dharmendra Singh. (2015). A review of transient and steady state response of DC Motor Position Control. International Journal of Engineering Research And, V4(06). https://doi.org/10.17577/ijertv4is060725
[7] Eid S. Mohamed and Saeed A. Albatlan. Modeling and Experimental Design Approach for Integration of Conventional Power Steering and a Steer-By-Wire System Based on Active Steering Angle Control. American Journal of Vehicle Design. 2014; 2(1):32-42. doi: 10.12691/ajvd-2-1-5